

# Impact of radiation dose and iterative reconstruction on pulmonary nodule measurements at chest CT: a phantom study

Hyungjin Kim  
Chang Min Park  
Hee-Dong Chae  
Sang Min Lee  
Jin Mo Goo

## PURPOSE

We aimed to identify the impact of radiation dose and iterative reconstruction (IR) on measurement of pulmonary nodules by chest computed tomography (CT).

## METHODS

CT scans were performed on a chest phantom containing various nodules (diameters of 3, 5, 8, 10, and 12 mm; +100, -630 and -800 HU for each diameter) at 80, 100, 120 kVp and 10, 20, 50, 100 mAs (a total of 12 radiation dose settings). Each CT was reconstructed using filtered back projection, iDose<sup>4</sup>, and iterative model reconstruction (IMR). Thereafter, two radiologists measured the diameter and attenuation of the nodules. Noise, contrast-to-noise ratio and signal-to-noise ratio of CT images were also obtained. Influence of radiation dose and reconstruction algorithm on measurement error and objective image quality metrics was analyzed using generalized estimating equations.

## RESULTS

The 80 kVp, 10 mAs CT scan was not feasible for the measurement of 3 mm sized simulated ground-glass nodule (GGN); otherwise, diameter measurement error was not significantly influenced by radiation dose ( $P > 0.05$ ). IR did not have a significant impact on diameter measurement error for simulated solid nodules ( $P > 0.05$ ). However, for simulated GGNs, IMR was associated with significantly decreased relative diameter measurement error ( $P < 0.001$ ). Attenuation measurement error was not significantly influenced by either radiation dose or reconstruction algorithm ( $P > 0.05$ ). Objective image quality was significantly better with IMR ( $P < 0.05$ ).

## CONCLUSION

Nodule measurements were not affected by radiation dose except for 3 mm simulated GGN on 80 kVp, 10 mAs dose setting. However, for GGNs, IMR may help reduce diameter measurement error while improving image quality.

Recently, the National Lung Screening Trial demonstrated that three annual low-dose computed tomography (CT) screenings (cumulative average effective dose, 4.5 mSv) resulted in a 20% relative mortality reduction of lung cancer in comparison with chest radiographs for individuals at high risk of lung cancer (1, 2). Despite the great advantage of low-dose CT screenings, one of the biggest considerations must be radiation exposure.

Currently, there are several techniques known to reduce radiation exposure from chest CT (3, 4). Modification of the tube current is the simplest method of radiation dose reduction and has been a mainstay of chest CT imaging for radiation dose reduction (5). As lowering radiation dose is often accompanied by increased noise in CT images reconstructed with the conventional filtered back projection (FBP) algorithm (6), noise-reducing iterative reconstruction (IR) algorithms have also become available. At present, all major CT vendors have their own unique IR techniques (6). A novel IR algorithm, iterative model reconstruction (IMR) (Philips Healthcare), was developed recently and this knowledge-based IR incorporates system optics as well as data statistics and image statistics.

For clinical application of these IR algorithms in conjunction with reduced radiation dose, the feasibility of lesion characterization and radiologic measurements are fundamental prerequisites. Nodule measurements should be performed equally well without significant variability between low-dose IR-applied CT images and standard-dose CT reconstructed with FBP. This is of great significance since the management of small incidentally-detected pulmonary nodules, especially ground-glass nodules (GGNs), differs based on nodule size

From the Department of Radiology (H.K., C.M.P.)  
✉ [cmpark@radiol.snu.ac.kr](mailto:cmpark@radiol.snu.ac.kr), H.D.C., S.M.L., J.M.G.),  
College of Medicine, and Institute of Radiation  
Medicine, Medical Research Center, Seoul National  
University, Seoul, Korea; Aerospace Medical Group  
(H.K.), Air Force Education and Training Command,  
Jinju, Korea; Cancer Research Institute (C.M.P.,  
J.M.G.), Seoul National University, Seoul, Korea.

Received 19 December 2014; revision requested 1  
February 2015; final revision received 19 March 2015;  
accepted 14 April 2015.

Published online 31 August 2015.  
DOI 10.5152/dir.2015.14541

and their changes over follow-up examinations (7). Manual measurements of nodule diameter on chest CT of various radiation doses from standard to ultra-low doses have been studied previously; however, the effect of IR algorithms were not considered in those investigations (8, 9). In addition, considering the fuzzy, ill-defined border of GGNs and the fact that GGNs are usually followed-up with low-dose CT, advantage of IR for the measurement of GGNs is clearly expected. Nevertheless, IR has not been highlighted for evaluating GGNs to date.

In this study, we hypothesized that the accuracy of manual nodule measurement would be potentially affected by various radiation dose settings and reconstruction algorithms such as iDose<sup>4</sup> (Philips Healthcare) and IMR. We suspected that the measurement of GGNs would be particularly influenced by the variables. Therefore, we performed modeling analysis using an anthropomorphic chest phantom with simulated nodules.

## Methods

The present study was exempt from Institutional Review Board approval of Seoul National University Hospital as no animal or human data were acquired or used.

### Phantom

To obtain CT scan images of various radiation doses, we performed a phantom study using an anthropomorphic male chest phantom (multipurpose chest phantom N1 Lungman, Kyoto Kagaku) with simulated pulmonary nodules (10–13). The anthropomorphic chest phantom consisted of simulated pulmonary vessels, heart, trachea, chest wall, diaphragm, and abdomen block. The phantom was made of polyurethane (soft tissue) and epoxy resin (synthetic bone). The phantom measured 43×40×48 cm in dimension with a chest girth of 94 cm. Simulated pulmonary nodules of various diameters and attenuations (diameter 3, 5, 8, 10 and 12 mm; attenuation +100, -630 and -800 HU for each diameter) were manually affixed to the simulated pulmonary vessels. Nodules with +100 HU simulated solid nodules and nodules with -630 and -800 HU simulated GGNs.

### CT acquisition

All CT scans were performed with a 256-section iCT scanner (Philips Healthcare). The phantom was scanned with a voltage of 80, 100, and 120 kVp and a tube current-time product of 10, 20, 50, and 100 mAs. Thus, a total of 12 radiation dose settings were used in this study (Table 1). Other acquisition parameters were as follows: detector collimation, 128×0.625 mm; gantry rotation time, 0.4 s; pitch, 0.915; FOV, 350 mm and matrix size, 512×512 pixels. All CT images were reconstructed with a slice thickness of 1 mm and an increment of 0.9 mm. The phantom was scanned once at each dose setting and all CT scans were obtained sequentially on the same day without changing the positions of either the phantom or the nodules within it.

### Iterative reconstruction techniques (iDose<sup>4</sup> and IMR)

A series of 12 CT scans at various radiation dose settings were reconstructed with FBP, iDose<sup>4</sup> (level 4) and IMR (level 1) algorithms. IR levels for iDose<sup>4</sup> and IMR were chosen empirically after preliminary review of CT images at each IR level to find a single IR level with optimum image quality. Thus, a total of 36 CT datasets were prepared (Fig. 1). A Y-Sharp (YA) filter was used for FBP and

iDose<sup>4</sup> and a sharp plus filter, as a possible YA-equivalent, was used for IMR, since YA could not be applied directly to IMR. iDose<sup>4</sup> is a hybrid iterative reconstruction algorithm and incorporates statistics-model based de-noising into raw and image data space (14). IMR is a novel knowledge-based iterative reconstruction algorithm and is an optimization process that incorporates knowledge of data statistics, image statistics, and system models (15). The notable feature of IMR is that the characteristics of the CT system such as detector sampling, angular sampling, and system geometries are taken into account in the optimization process (15). Consideration of the system properties allow for design of the cost function, allowing IMR to effectively control image noise while maximizing spatial resolution at radiation doses that are significantly lower than those traditionally used with FBP reconstruction (15).

### Radiation dose assessment

For radiation dose assessment, the volume CT dose index (CTDI<sub>vol</sub>) and dose-length product (DLP) were recorded at each kVp and mAs. CTDI<sub>vol</sub> and DLP were acquired from the dose information provided by the CT scanner. Estimated effective dose was calculated from the DLP using a conversion factor of 0.0145 according to the International Commission on Radiological Protection publication 103 recommendations (16). Dose reduction in percentages was calculated compared with the radiation dose of a 120 kVp and 100 mAs CT scan (Table 1).

### Measurement of nodule diameter and attenuation

Two radiologists (H.K. and H.D.C., with four and three years of experience in chest

### Main points

- Simulated pulmonary nodule diameter measurement error is not significantly affected by the radiation dose.
- Iterative reconstruction algorithms do not have a significant impact on diameter measurement error for simulated solid nodules.
- Iterative model reconstruction (IMR) can help reduce the measurement error of ground-glass nodules.
- IMR provides better image quality in terms of image noise, contrast-to-noise ratio and signal-to-noise ratio.

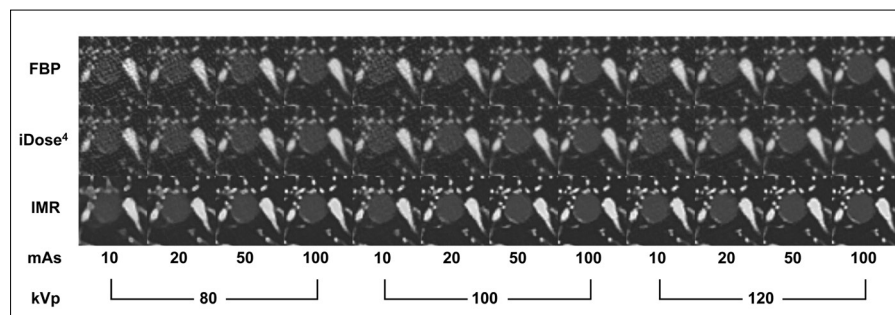


**Figure 1.** A -800 HU, 12 mm nodule scanned at various radiation dose protocols and iterative reconstruction algorithms. Noise is remarkably reduced in IMR-applied images, leading to improved nodule margin delineation and decreased relative diameter measurement error by the radiologists. FBP, filtered back projection; IMR, iterative model reconstruction.

CT, respectively), who were blinded to the size and attenuation of simulated nodules, independently performed measurements of maximum diameter and internal attenuation of the nodules at picture archiving and communication system (PACS) of our hospital (Maroview, Infinitt). Maximum diameter was measured manually using an electronic caliper in the fixed lung window setting (window width, 1600 HU; window level, -600 HU) and internal attenuation was measured by placing a circular region of interest (ROI) within each phantom nodule. To avoid misregistration due to small nodule size, attenuation measurements were performed only for 8, 10, and 12 mm nodules. The areas of ROI were 21, 32, and 44 mm<sup>2</sup>, respectively. Magnification of CT images using the zoom function of PACS was allowed for the measurements.

### Objective image quality assessment

To assess the image quality of CT scans, the standard deviations (SD) of attenuation in the two different simulated lung fields (left posterolateral lung field near the chest wall and right anteromedial lung field near the mediastinum at the level of the heart) and in the air outside the chest wall (approximately 3 cm away from the middle anterior chest wall at the level of the heart) were measured. As the chest phantom did not have a true lung parenchyma, the simulated lung fields were actually air in the phantom. These three SD values were averaged to calculate the noise of each CT scan. The area of ROI was 198 mm<sup>2</sup>.

In addition, contrast-to-noise ratio (CNR) was calculated by each reader using the following equation:  $CNR = \frac{\text{Attenuation of the nodule} - \text{Attenuation of the background lung field}}{SD \text{ of the background lung field}}$ . Signal-to-noise ratio (SNR) was also calculated by each reader using the following equation:  $SNR = \frac{\text{Attenuation of the nodule}}{SD \text{ of the nodule}}$ . The nodule of -800 HU and 12 mm was chosen for CNR and SNR analyses, as this simulated nodule was of the lowest lesion-to-background contrast and CNR and SNR are important metrics especially for evaluation of low contrast lesions. Simulated vessels were carefully avoided from the ROIs of the background lung field.

### Statistical analysis

A series of generalized estimating equations (GEE) models with an exchangeable correlation structure were performed to

test the associations between nodule size, nodule type, radiation dose, and reconstruction algorithm on changes in the relative measurement error of the simulated nodules. This approach takes into account

clustered data of 15 nodule datasets imaged at multiple radiation dose settings and IR algorithms. The GEE model was run with the relative measurement error of diameter as an dependent variable and nod-

**Table 1.** Descriptive statistics for radiation dose protocols

Tube voltage (kVp)	Tube current-time product (mAs)	CTDI <sub>vol</sub> (mGy)	DLP (mGy-cm)	ED <sup>a</sup> (mSv)	Dose reduction <sup>b</sup> (%)
80	10	0.20	7.8	0.11	97.1
	20	0.38	15.3	0.22	94.3
	50	0.97	38.6	0.56	85.6
100	10	1.95	77.6	1.13	71.1
	20	4.04	161.0	2.34	40.0
	50	6.74	268.5	3.89	0
120	10	0.41	16.2	0.24	94.0
	20	0.81	32.3	0.47	88.0
	50	2.01	80.1	1.16	70.2
120	10	0.68	27.0	0.39	89.9
	20	1.32	52.8	0.77	80.3
	50	3.38	134.8	1.96	49.8
120	100	6.74	268.5	3.89	0

<sup>a</sup>Conversion factor of 0.0145 was used for the estimation of ED (16).

<sup>b</sup>Dose reduction of each CT scan was calculated compared to 120 kVp and 100 mAs acquisition.

CTDI<sub>vol</sub>, volume CT dose index; DLP, dose-length product; ED, effective dose.

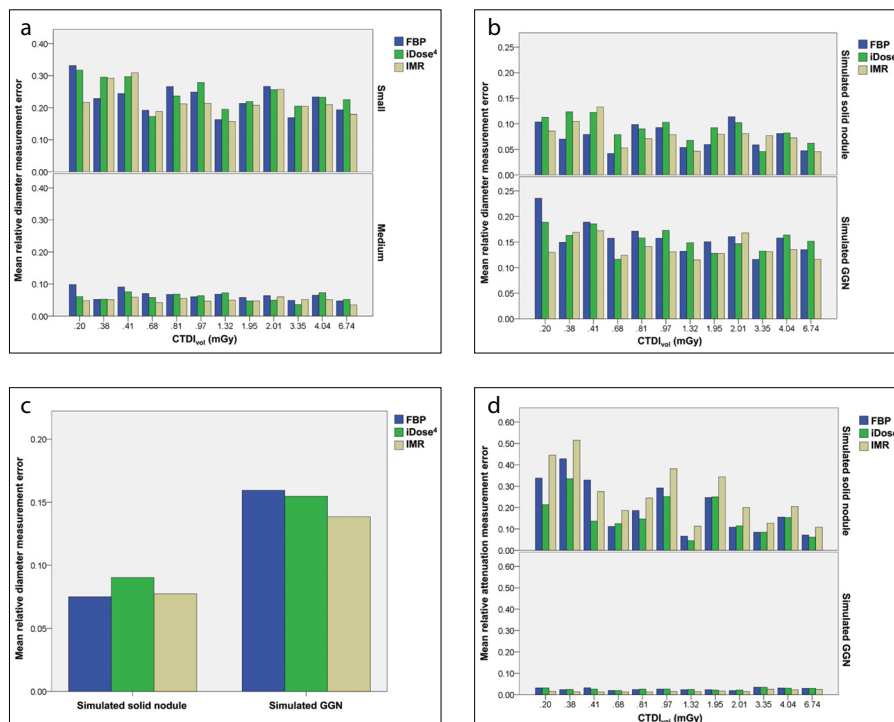


**Figure 2. a–d.** Mean relative diameter measurement error was significantly larger in small nodules (3 and 5 mm) than in medium sized nodules (8, 10, and 12 mm) (a). Mean relative measurement error was also significantly larger in simulated GGNs (-630, -800 HU) than in solid (+100 HU) nodules (b). IMR was associated with significant decrease in measurement error in GGNs (c). Mean relative attenuation measurement error was significantly larger in simulated solid nodules (+100 HU) than in GGNs (-630, -800 HU) (d). FBP, filtered back projection; GGN, ground-glass nodule; HU, Hounsfield unit; IMR, iterative model reconstruction.

ule size, nodule type, radiation dose, and reconstruction algorithm as independent variables. CNR and SNR were not included in the GEE models as they were consequences of radiation dose and reconstruction algorithms, not fundamental factors. For relative attenuation measurement error, the same independent variables were used except for nodule size, as nodules of similar diameter (8, 10, and 12 mm) were measured. The initial GEE models were run with main effects terms with entry of interaction terms iteratively. Then, the final GEE model was run with statistically significant main effects terms and interaction terms. Nodule size was classified into two groups of small (3 and 5 mm) and medium (8, 10, and 12 mm) sizes. Nodule type was also categorized into two groups of solid nodules (+100 HU) and GGNs (-630 and -800 HU). For radiation dose, CTDI<sub>vol</sub> was used. Reconstruction algorithms included FBP, iDose<sup>4</sup>, and IMR. The dependent variable of relative measurement error was calculated as follows: (Measured nodule diameter or attenuation - Reference nodule diameter or attenuation) / Reference nodule diameter or attenuation. Data of both readers were used in the analyses.

For objective image quality assessment, GEE modeling was also performed as described above with noise, CNR, and SNR as dependent variables, and radiation dose and reconstruction algorithm as independent variables. Data of both readers were used in the analyses.

Interobserver agreement of the measured values was evaluated using the Bland-Altman plot and Lin's concordance

correlation coefficient ( $\rho_c$ ). Comparisons were performed pairwise on a reconstruction algorithm-to-reconstruction algorithm basis. For the Bland-Altman plot, relative differences in measurements were calculated as the difference between the two measurements divided by the mean. Then, interobserver variability was defined as a 95% confidence interval (CI) of the relative differences (17). For Lin's concordance correlation coefficient, poor agreement was defined as  $\rho_c < 0.90$ , whereas higher  $\rho_c$  values represented moderate ( $0.90 \leq \rho_c < 0.95$ ), good ( $0.95 \leq \rho_c < 0.99$ ), or excellent ( $\rho_c > 0.99$ ) agreement (18, 19).

All statistical analyses were performed using SAS version 9.2 (SAS Institute Inc.) and MedCalc version 12.3.0 (MedCalc Software). A *P* value  $< 0.05$  was considered to indicate a statistical significance.

## Results

Reader 1 reported that the diameter measurement of the -800 HU, 3 mm nodule was not available on the 80 kVp, 10 mAs scan due to an ill-defined nodule margin regardless of the reconstruction algorithm. Reader 1 also reported that the margin of the -630 HU, 3 mm nodule on the 80 kVp, 10 mAs scan reconstructed using IMR was not distinguishable from the background. Therefore, these four measurements by reader 1 were not included in statistical analyses. Detailed data regarding the mean and CI of relative diameter measurement error according to nodule size, nodule type, radiation dose, and reconstruction algorithm are listed in supplemental Tables 1 and 2.

In the initial GEE models, radiation dose showed no significant association with relative diameter measurement error ( $P > 0.05$ ), and thus it was excluded from the model. Among the multiple interaction terms, the interaction between nodule type and reconstruction algorithm showed a statistical significance ( $P = 0.042$ ), and thus it was included in the model. The final GEE model revealed that the nodule type of GGNs (-630 and -800 HU;  $\beta = 0.09$ ,  $P = 0.018$ ) and small nodule size (3 and 5 mm;  $\beta = 0.18$ ,  $P < 0.001$ ) were associated with increased relative diameter measurement error (Fig. 2a, 2b). For solid nodules (+100 HU), IMR was associated with decreased relative diameter measurement error compared with iDose<sup>4</sup> ( $\beta = -0.01$ ,  $P = 0.047$ ). However, for iDose<sup>4</sup> compared with FBP or IMR compared with FBP, the association between relative diameter measurement error and reconstruction algorithm was not significant (iDose<sup>4</sup> vs. FBP,  $P = 0.249$ ; IMR vs. FBP,  $P = 0.739$ ). For GGNs (-630 and -800 HU), IMR was associated with decreased relative diameter measurement error compared with FBP ( $\beta = -0.02$ ,  $P < 0.001$ ) and compared with iDose<sup>4</sup> ( $\beta = -0.02$ ,  $P < 0.001$ ) (Fig. 2c); however, iDose<sup>4</sup> was not significantly different compared with FBP ( $P = 0.375$ ). *P* values of GEE models are listed in detail in supplemental Table 3. Detailed data regarding the mean and CI of relative attenuation measurement error according to nodule type, radiation dose, and reconstruction algorithm are listed in supplemental Table 4.

Radiation dose and reconstruction algorithm did not show any significant association with changes in relative attenuation measurement error (all  $P > 0.05$ ). There were no significant interactions among variables (all  $P > 0.05$ ). Therefore, the GEE model was run with the independent variable of nodule type. GGNs (-630 and -800 HU;  $\beta = -0.19$ ,  $P < 0.001$ ) were associated with decreased relative attenuation measurement error (Fig. 2d). *P* values of GEE models are listed in detail in supplemental Table 5.

As for image noise, CNR, and SNR, the initial GEE model revealed that the radiation dose by reconstruction algorithm interaction was significant (all  $P < 0.001$ ). Thus, the final GEE model was run with radiation dose, reconstruction algorithm, and radiation dose by reconstruction algorithm interaction.

An increase in radiation dose was significantly associated with a decrease in image noise at all radiation dose settings (refer-

**Table 2.** Interobserver measurement variability

Measurement		FBP	iDose <sup>4</sup>	IMR
Diameter	Interobserver variability <sup>a</sup>	-24.2, 10.0	-24.1, 8.7	-26.6, 13.4
	$\rho_c$	0.98	0.97	0.98
Attenuation	Interobserver variability <sup>a</sup>	-10.9, 12.3	-7.5, 6.8	-5.2, 4.8
	$\rho_c$	1.00	1.00	1.00
Noise	Interobserver variability <sup>a</sup>	-5.1, 4.1	-1.5, 1.9	-6.6, 5.3
	$\rho_c$	1.00	1.00	0.98
CNR	Interobserver variability <sup>a</sup>	-16.8, 11.4	-7.5, 7.4	-5.4, 7.3
	$\rho_c$	1.00	1.00	0.98
SNR	Interobserver variability <sup>a</sup>	-13.5, 12.1	-14.1, 10.5	-12.8, 16.3
	$\rho_c$	0.99	0.99	0.92

<sup>a</sup>The results of Bland-Altman analyses are displayed in 95% confidence interval of the relative differences in percentage.  $\rho_c$ , concordance correlation coefficient; FBP, filtered back projection; IMR, iterative model reconstruction; CNR, contrast-to-noise ratio; SNR, signal-to-noise ratio.

ence dose, 0.2 mGy) for all three reconstruction algorithms, except for 0.41 over 0.20 mGy at IMR ( $P = 0.054$ ) (Fig. 3a). The reduction in image noise according to reconstruction algorithm was significant at all radiation dose settings ( $P < 0.001$  for iDose<sup>4</sup> vs. FBP, IMR vs. FBP, and IMR vs. iDose<sup>4</sup>).

An increase in radiation dose was also significantly associated with an increase in CNR at all radiation dose settings (reference dose, 0.2 mGy) for all three reconstruction algorithms, except for 0.41 over 0.20 mGy at IMR ( $\beta = -0.82$ ,  $P < 0.001$ ) (Fig. 3b). The increase in CNR according to reconstruction algorithm was significant at all radiation dose settings ( $P < 0.001$  for iDose<sup>4</sup> vs. FBP, IMR vs. FBP, and IMR vs. iDose<sup>4</sup>).

Likewise, an increase in radiation dose was significantly associated with an increase in SNR at all radiation dose settings (reference dose, 0.2 mGy) of all three reconstruction algorithms except for 0.81 over 0.20 mGy at IMR ( $P = 0.589$ ) (Fig. 3c). The increase in SNR according to reconstruction algorithm (iDose<sup>4</sup> vs. FBP, IMR vs. FBP, and IMR vs. iDose<sup>4</sup>) was significant at all radiation dose settings (all  $P < 0.001$ ).

The results of Bland-Altman analysis and concordance correlation coefficients are listed in Table 2. Interobserver agreement for measuring diameter, attenuation, noise, CNR, and SNR was good to excellent (all  $\rho_c > 0.97$ ) except for the SNR measurement at IMR ( $\rho_c = 0.92$ ).

## Discussion

We found that the nodule diameter measurement error was not significantly influenced by radiation dose except for the 3 mm simulated GGN on 80 kVp, 10 mAs dose setting. For simulated solid nodules, IR algorithms did not have a significant impact

on diameter measurement error compared with FBP. However, for simulated GGNs, IMR was shown to be significantly associated with decreased relative nodule diameter measurement error. Finally, IMR was shown to have significantly better image quality in terms of image noise, CNR, and SNR.

There have been several studies which have dealt with multiple radiation dose settings and tumor measurements (8, 9). Hein et al. (9) performed two CT scans for each patient at different radiation doses (120 kV, 5 mAs and 120 kV, 75 mAs), and concluded that the mean relative differences did not significantly differ between measurements from 120 kV, 5 mAs CT and those from 120 kV, 75 mAs CT (9). On the contrary, Christie et al. (8) reported contradictory results showing that the manual diameter measurement exhibits significant differences with lower tube current-time levels of 100 mAs or less. However, all CT scans in their study were performed using 120 kVp, 300 mAs and were artificially reconstructed with noise superimposing software to simulate multiple radiation dose levels. In addition, the included nodules were of very small size. The mean nodule diameter was 2.11 mm and ranged from 1.1–8.0 mm (8). In our study, the nodule diameter measurement was not affected by radiation dose settings. Our finding is meaningful in that diameter measurement is feasible even when radiation dose is substantially reduced. Serial follow-up CT scans are required for cancer patients undergoing chemotherapy to evaluate tumor response and to decide whether to continue or discontinue the chemotherapy. It is also required for patients with indeterminate nodules so as to decide whether or not to conservatively follow-up these patients. These patients are expected to benefit from ultra-low dose

CT without losing measurement accuracy. Nevertheless, we do not believe that an 80 kVp, 10 mAs scan (CTDI<sub>vol</sub> 0.20 mGy, the lowest dose in this study protocol) is the suitable CT protocol for either initial screening or follow-up. As stated in the study results, reader 1 reported that the diameter measurement of the -800 HU, 3 mm nodule was not available on this radiation dose due to the severely blurred nodule margin. Reader 1 also reported that the margin of the -630 HU, 3 mm nodule on the 80 kVp, 10 mAs scan reconstructed using IMR was not distinguishable from the background. Considering the observed loss of detectability, the 80 kVp, 10 mAs scan may not be feasible for the evaluation of small GGNs.

Studies regarding semiautomatic volumetric analysis of lung nodules showed that nodule volumes measured with IR were comparable to those with standard FBP (11, 18, 20). Although manual measurements cannot be directly compared with semiautomatic computer-aided volumetry, these studies imply that the nodule margin characteristics on CT scans reconstructed using an IR algorithm are at the least not deteriorated. Our study demonstrated that the human delineation of the nodule margin was not significantly influenced by the reconstruction algorithm used. Rather, the measurement accuracy of GGNs in IMR-applied CT scans improved significantly, compared with that of FBP- or iDose<sup>4</sup>-applied CT scans. As GGNs are low contrast lesions, improvement in lesion margin delineation on CT scans reconstructed with IMR may help radiologists to detect and follow-up GGNs in a more reproducible manner. In future, *in vivo* measurement variability studies are warranted to validate our findings.

Regarding the increased diameter measurement error of small nodules, our re-

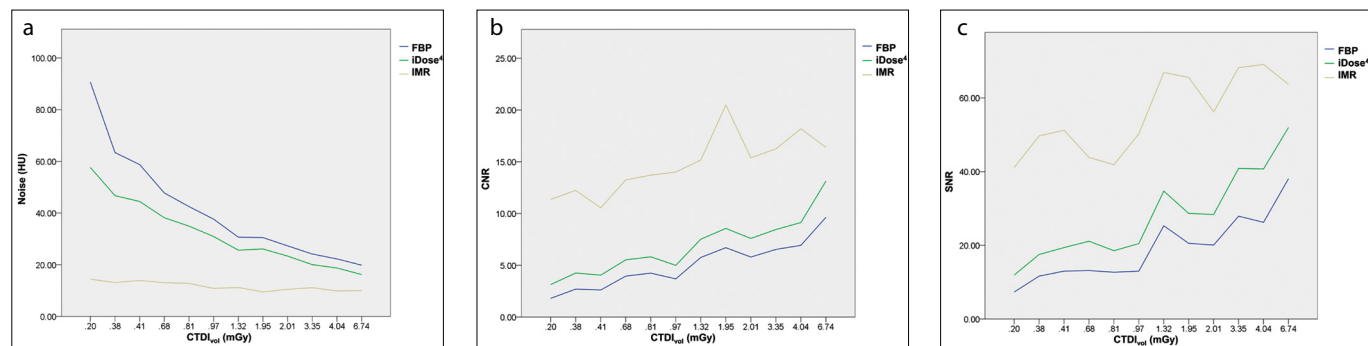


**Figure 3.** a–c. Image noise in IMR was constantly lower than the noise in other reconstruction algorithms at all radiation dose settings (a). Contrast-to-noise ratio (CNR, b) and signal-to-noise ratio (SNR, c) in IMR were constantly higher than those in other reconstruction algorithms. FBP, filtered back projection; IMR, iterative model reconstruction.

sults are consistent with previous reports (21). Oxnard et al. (21) revealed that the relative measurement change (percent increase or percent decrease) was found to be significantly larger for smaller tumors. Considering that the variability range of a 2 cm nodule was 1.6–2.4 cm and that of a 4 cm nodule was 3.5–4.5 cm in that study (21), the measurement variability would be much higher for 3 mm and 5 mm nodules, which in turn would increase the relative measurement error. As for measurement accuracy related to the nodule type, it is plausible that GGNs are associated with increased diameter measurement error, given that the simulated GGNs have far lower lesion-to-background contrast than simulated solid nodules. In the clinical setting, some GGNs even show the fade-out pattern of their nodule margin which would aggravate the measurement accuracy and reproducibility.

As IR algorithms have clear merits of reducing image noise and artifacts in low-dose CT scans, many researchers are now paying close attention to the clinical usefulness of IR. To date, many studies have focused on image quality assessment and dose reduction in regards to IR as these are the most important issues. Our study also showed the improved image quality of IR-applied CT scans from the aspect of image noise, CNR, and SNR. In addition, at all radiation dose settings, IMR significantly improved image noise, CNR, and SNR compared to FBP and iDose<sup>4</sup>. In addition, the overall magnitude of improvement in CNR and SNR from switching reconstruction algorithm (FBP to IMR) at each dose level was much higher than that caused by radiation dose increment at each dose level when compared with the lowest radiation dose (FBP), as displayed on Fig. 3b, 3c. This fact would partially explain our study result that only IMR, not the radiation dose, was associated with the improvement in measurement accuracy of simulated GGNs.

Thus far, the reported achieved radiation dose reductions with IR have varied widely from 23% to 76%, with preserved image quality (22). Katsura et al. (23) even reported that IR (model-based iterative reconstruction) enabled nearly 80% reduction in radiation dose at chest CT from a low dose level to an ultra-low dose level, without affecting nodule detectability. In our study, we showed that tumor measurements were feasible in further reduced dose settings of approximately 0.2 mSv (80 kVp, 20 mAs).

Issues regarding lesion detection and characterization still remain for this dose setting with IMR application.

In our study, several potential limitations merit consideration. First, the results obtained from a phantom study cannot be directly applied to patients. This is partly because simulated nodules used in the phantom study might be overly simplistic as the simulated nodules were completely spherical in shape with homogeneous radiodensity. Also, noise can be artificially low with IR in a homogeneous phantom since IR can reduce noise more prominently in homogeneous tissue than in inhomogeneous tissue (6). Furthermore, the lack of true lung parenchyma in the chest phantom may have contributed to increased measurement reproducibility and CNR. Second, the number of nodules in our study was relatively small and thus further prospective studies with a larger number of pulmonary nodules are warranted. Third, our results regarding IR algorithm are vendor specific. Other newly developed IR algorithms from major vendors should be studied as well. Fourth, we did not deal with nodule detectability according to dose reduction in the current study and this issue should be investigated in subsequent *in vivo* studies. Fifth, the image filters used for each reconstruction algorithm were different (Y-Sharp for FBP and iDose<sup>4</sup>; sharp plus filter for IMR) and their equivalence or potential impact on image quality assessment was not tested. Those filters are used for lung imaging and were chosen empirically after the preliminary review of images. Sixth, we did not evaluate the interobserver variability of diameter measurement according to nodule size as this issue was beyond the primary purpose of our study. However, we admit that the lack of thorough investigation of measurement variability would be a limitation of our study as it is an important performance metric.

In conclusion, our study demonstrated that nodule diameter measurement error was not significantly influenced by radiation dose except for 3 mm simulated GGN on 80 kVp, 10 mAs dose setting. IR algorithms did not have a significant impact on diameter measurement error compared with FBP for simulated solid nodules. However, for simulated GGNs, IMR was shown to be associated with decreased relative nodule diameter measurement error, while significantly improving image noise, CNR, and SNR.

## Acknowledgements

We acknowledge Youngmi Chun and Jae Young Cho for their help in image acquisition. We would like to express special thanks to the Medical Research Collaborating Center in Seoul National University Hospital for help on statistical analyses.

This study was supported by the Research Grant of the Korean Foundation for Cancer Research (grant number: CB-2011-02-01). The funding source had no involvement in the study design; in the collection, analysis and interpretation of data; in the writing of the report; and in the decision to submit the paper for publication.

## Conflict of interest disclosure

The authors declared no conflicts of interest.

## References

1. Bach PB, Mirkin JN, Oliver TK, et al. Benefits and harms of CT screening for lung cancer: a systematic review. *JAMA* 2012; 307:2418–2429. [CrossRef]
2. Aberle DR, Adams AM, Berg CD, et al. Reduced lung-cancer mortality with low-dose computed tomographic screening. *N Engl J Med* 2011; 365:395–409. [CrossRef]
3. McCollough CH, Chen GH, Kalender W, et al. Achieving routine submillisievert CT scanning: report from the summit on management of radiation dose in CT. *Radiology* 2012; 264:567–580. [CrossRef]
4. Litmanovich DE, Tack DM, Shahrzad M, Bankier AA. Dose reduction in cardiothoracic CT: review of currently available methods. *Radiographics* 2014; 34:1469–1489. [CrossRef]
5. Kubo T, Lin PJ, Stiller W, et al. Radiation dose reduction in chest CT: a review. *AJR Am J Roentgenol* 2008; 190:335–343. [CrossRef]
6. Willeminck MJ, de Jong PA, Leiner T, et al. Iterative reconstruction techniques for computed tomography Part 1: technical principles. *Eur Radiol* 2013; 23:1623–1631. [CrossRef]
7. MacMahon H, Austin JH, Gamsu G, et al. Guidelines for management of small pulmonary nodules detected on CT scans: a statement from the Fleischner Society. *Radiology* 2005; 237:395–400. [CrossRef]
8. Christe A, Torrente JC, Lin M, et al. CT screening and follow-up of lung nodules: effects of tube current-time setting and nodule size and density on detectability and of tube current-time setting on apparent size. *AJR Am J Roentgenol* 2011; 197:623–630. [CrossRef]
9. Hein PA, Romano VC, Rogalla P, et al. Linear and volume measurements of pulmonary nodules at different CT dose levels - intrascan and interscan analysis. *Rofo* 2009; 181:24–31. [CrossRef]
10. Coenen A, Honda O, van der Jagt EJ, Tomiyama N. Computer-assisted solid lung nodule 3D volumetry on CT: influence of scan mode and iterative reconstruction: a CT phantom study. *Jpn J Radiol* 2013; 31: 677–684. [CrossRef]
11. Willeminck MJ, Leiner T, Budde RP, et al. Systematic error in lung nodule volumetry: effect of iterative reconstruction versus filtered back projection at different CT parameters. *AJR Am J Roentgenol* 2012; 199:1241–1246. [CrossRef]
12. Xie X, Zhao Y, Snijder RA, et al. Sensitivity and accuracy of volumetry of pulmonary nodules on low-dose 16- and 64-row multi-detector CT: an anthropomorphic phantom study. *Eur Radiol* 2013; 23:139–147. [CrossRef]

13. Kim H, Park CM, Lee SM, Lee HJ, Goo JM. A comparison of two commercial volumetry software programs in the analysis of pulmonary ground-glass nodules: segmentation capability and measurement accuracy. *Korean J Radiol* 2013; 14:683–691. [\[CrossRef\]](#)
14. Funama Y, Taguchi K, Utsunomiya D, et al. Combination of a low-tube-voltage technique with hybrid iterative reconstruction (iDose) algorithm at coronary computed tomographic angiography. *J Comput Assist Tomogr* 2011; 35:480–485. [\[CrossRef\]](#)
15. Mehta D, Thompson R, Morton T, Dhanantwari A, Shefer E. Iterative model reconstruction: simultaneously lowered computed tomography radiation dose and improved image quality. *Med Phys Int* 2013; 1:147–155.
16. Deak PD, Smal Y, Kalender WA. Multisection CT protocols: sex- and age-specific conversion factors used to determine effective dose from dose-length product. *Radiology* 2010; 257:158–166. [\[CrossRef\]](#)
17. Bland JM, Altman DG. Measuring agreement in method comparison studies. *Stat Methods Med Res* 1999; 8:135–160. [\[CrossRef\]](#)
18. Willemink MJ, Borstlap J, Takx RA, et al. The effects of computed tomography with iterative reconstruction on solid pulmonary nodule volume quantification. *PLoS One* 2013; 8:e58053. [\[CrossRef\]](#)
19. Lin LI. A concordance correlation coefficient to evaluate reproducibility. *Biometrics* 1989; 45:255–268. [\[CrossRef\]](#)
20. Xu Y, He W, Chen H, Hu Z, Li J, Zhang T. Impact of the adaptive statistical iterative reconstruction technique on image quality in ultra-low-dose CT. *Clin Radiol* 2013; 68:902–908. [\[CrossRef\]](#)
21. Oxnard GR, Zhao B, Sima CS, et al. Variability of lung tumor measurements on repeat computed tomography scans taken within 15 minutes. *J Clin Oncol* 2011; 29:3114–3119. [\[CrossRef\]](#)
22. Willemink MJ, Leiner T, de Jong PA, et al. Iterative reconstruction techniques for computed tomography part 2: initial results in dose reduction and image quality. *Eur Radiol* 2013; 23:1632–1642. [\[CrossRef\]](#)
23. Katsura M, Matsuda I, Akahane M, et al. Model-based iterative reconstruction technique for ultralow-dose chest CT: comparison of pulmonary nodule detectability with the adaptive statistical iterative reconstruction technique. *Invest Radiol* 2013; 48:206–212. [\[CrossRef\]](#)

**Supplemental Table 1. Relative diameter measurement error according to the nodule size, various radiation dose protocols, and IR algorithms**

CTDI <sub>vol</sub> (mGy)	Small (3, 5 mm)						Medium (8, 10, 12 mm)					
	FBP		iDose <sup>4</sup>		IMR		FBP		iDose <sup>4</sup>		IMR	
	Mean <sup>a</sup>	95% CI	Mean <sup>a</sup>	95% CI	Mean <sup>a</sup>	95% CI	Mean <sup>a</sup>	95% CI	Mean <sup>a</sup>	95% CI	Mean <sup>a</sup>	95% CI
0.20	0.36±0.24	0.20, 0.52	0.35±0.19	0.22, 0.48	0.26±0.18	0.13, 0.39	0.10±0.07	0.06, 0.13	0.06±0.05	0.04, 0.09	0.05±0.04	0.03, 0.07
0.38	0.23±0.15	0.13, 0.33	0.30±0.17	0.19, 0.40	0.29±0.19	0.17, 0.41	0.05±0.04	0.04, 0.07	0.05±0.04	0.03, 0.07	0.05±0.04	0.03, 0.07
0.41	0.24±0.19	0.13, 0.363	0.30±0.19	0.18, 0.42	0.31±0.20	0.18, 0.43	0.09±0.07	0.05, 0.13	0.08±0.05	0.05, 0.10	0.06±0.05	0.04, 0.08
0.68	0.19±0.16	0.09, 0.30	0.17±0.18	0.06, 0.29	0.19±0.17	0.08, 0.30	0.07±0.07	0.03, 0.11	0.06±0.05	0.03, 0.08	0.04±0.04	0.03, 0.06
0.81	0.27±0.18	0.16, 0.38	0.25±0.17	0.13, 0.35	0.21±0.14	0.12, 0.30	0.07±0.06	0.04, 0.10	0.07±0.05	0.04, 0.10	0.06±0.04	0.04, 0.07
0.97	0.25±0.13	0.17, 0.33	0.28±0.17	0.17, 0.38	0.21±0.12	0.14, 0.29	0.06±0.05	0.04, 0.09	0.06±0.04	0.04, 0.09	0.05±0.03	0.03, 0.06
1.32	0.16±0.16	0.06, 0.27	0.20±0.16	0.10, 0.29	0.16±0.16	0.05, 0.26	0.07±0.05	0.04, 0.10	0.07±0.05	0.05, 0.10	0.05±0.05	0.02, 0.08
1.95	0.21±0.16	0.11, 0.32	0.22±0.15	0.13, 0.31	0.21±0.16	0.11, 0.31	0.06±0.04	0.04, 0.08	0.05±0.04	0.03, 0.07	0.05±0.04	0.03, 0.07
2.01	0.27±0.17	0.16, 0.38	0.26±0.17	0.15, 0.36	0.26±0.19	0.14, 0.38	0.06±0.05	0.04, 0.09	0.05±0.04	0.03, 0.07	0.06±0.04	0.04, 0.08
3.35	0.17±0.16	0.07, 0.27	0.21±0.19	0.09, 0.32	0.20±0.17	0.09, 0.32	0.05±0.05	0.03, 0.07	0.04±0.03	0.02, 0.05	0.05±0.04	0.03, 0.07
4.04	0.23±0.20	0.11, 0.36	0.23±0.21	0.10, 0.36	0.21±0.19	0.09, 0.33	0.07±0.06	0.04, 0.09	0.07±0.05	0.05, 0.10	0.05±0.04	0.03, 0.07
6.74	0.20±0.16	0.09, 0.29	0.23±0.18	0.11, 0.34	0.18±0.13	0.10, 0.26	0.05±0.05	0.03, 0.07	0.05±0.04	0.03, 0.07	0.04±0.03	0.00, 0.05

<sup>a</sup>Data are presented as mean±standard deviation.  
IR, iterative reconstruction; CTDI<sub>vol</sub>, volume CT dose index; FBP, filtered back projection; IMR, iterative model reconstruction; CI, confidence interval.

**Supplemental Table 2. Relative diameter measurement error according to the nodule type, various radiation dose protocols, and IR algorithms**

CTDI <sub>vol</sub> (mGy)	Simulated solid nodule (+100 HU)						Simulated GGN (-630, -800 HU)					
	FBP		iDose <sup>4</sup>		IMR		FBP		iDose <sup>4</sup>		IMR	
	Mean <sup>a</sup>	95% CI	Mean <sup>a</sup>	95% CI	Mean <sup>a</sup>	95% CI	Mean <sup>a</sup>	95% CI	Mean <sup>a</sup>	95% CI	Mean <sup>a</sup>	95% CI
0.20	0.10±0.12	0.02, 0.19	0.11±0.17	-0.01, 0.23	0.09±0.12	-0.00, 0.17	0.24±0.22	0.14, 0.35	0.20±0.19	0.11, 0.29	0.15±0.16	0.06, 0.23
0.38	0.07±0.08	0.02, 0.13	0.12±0.17	0.00, 0.24	0.11±0.19	-0.03, 0.24	0.15±0.15	0.08, 0.22	0.16±0.16	0.09, 0.24	0.17±0.16	0.10, 0.24
0.41	0.08±0.09	0.02, 0.14	0.12±0.17	0.00, 0.24	0.13±0.16	0.02, 0.25	0.19±0.16	0.11, 0.26	0.19±0.16	0.11, 0.26	0.17±0.19	0.09, 0.26
0.68	0.04±0.05	0.01, 0.08	0.08±0.11	0.00, 0.16	0.05±0.05	0.02, 0.09	0.16±0.14	0.09, 0.22	0.12±0.14	0.05, 0.18	0.12±0.15	0.05, 0.20
0.81	0.10±0.12	0.01, 0.19	0.09±0.11	0.01, 0.17	0.07±0.11	-0.01, 0.15	0.17±0.16	0.10, 0.25	0.16±0.15	0.09, 0.23	0.14±0.12	0.08, 0.20
0.97	0.09±0.09	0.03, 0.16	0.10±0.14	0.00, 0.21	0.08±0.09	0.02, 0.14	0.16±0.14	0.09, 0.22	0.17±0.15	0.10, 0.25	0.13±0.12	0.07, 0.19
1.32	0.05±0.05	0.02, 0.09	0.07±0.05	0.03, 0.11	0.05±0.04	0.02, 0.08	0.13±0.13	0.70, 0.20	0.15±0.14	0.09, 0.21	0.12±0.14	0.05, 0.18
1.95	0.06±0.07	0.01, 0.11	0.09±0.12	0.01, 0.18	0.08±0.11	0.00, 0.16	0.15±0.14	0.08, 0.22	0.13±0.14	0.06, 0.19	0.13±0.14	0.06, 0.19
2.01	0.11±0.15	0.01, 0.22	0.10±0.12	0.02, 0.19	0.08±0.11	0.01, 0.16	0.16±0.15	0.09, 0.23	0.15±0.16	0.07, 0.22	0.17±0.17	0.09, 0.25
3.35	0.06±0.07	0.01, 0.11	0.05±0.04	0.02, 0.08	0.08±0.08	0.02, 0.14	0.12±0.14	0.05, 0.18	0.13±0.17	0.05, 0.21	0.13±0.15	0.06, 0.20
4.04	0.08±0.11	0.01, 0.16	0.08±0.11	0.01, 0.16	0.07±0.11	-0.01, 0.15	0.16±0.17	0.08, 0.24	0.16±0.17	0.08, 0.24	0.14±0.16	0.06, 0.21
6.74	0.05±0.05	0.01, 0.08	0.06±0.08	0.01, 0.12	0.05±0.05	0.01, 0.08	0.14±0.14	0.07, 0.20	0.15±0.16	0.08, 0.23	0.12±0.13	0.06, 0.18

<sup>a</sup>Data are presented as mean±standard deviation.  
IR, iterative reconstruction; HU, Hounsfield unit; GGN, ground-glass nodule; CTDI<sub>vol</sub>, volume CT dose index; FBP, filtered back projection; IMR, iterative model reconstruction; CI, confidence interval.

Supplemental Table 3. Generalized estimating equations model for the relative diameter measurement error

	Model number	Independent variable	P	Comparison detail
Initial model	1	Nodule size	0.007 <sup>a</sup>	
		Nodule type	0.092	
		Radiation dose	0.278	
		Reconstruction algorithm	0.022 <sup>a</sup>	
		Radiation dose* Reconstruction algorithm	0.451	
	2	Nodule size	0.009 <sup>a</sup>	
		Nodule type	0.091	
		Radiation dose	0.508	
		Reconstruction algorithm	0.005 <sup>a</sup>	
		Radiation dose*Nodule size	0.298	
	3	Nodule size	0.008 <sup>a</sup>	
		Nodule type	0.093	
		Radiation dose	0.416	
		Reconstruction algorithm	0.005 <sup>a</sup>	
		Radiation dose*Nodule type	0.550	
	4	Nodule size	0.010 <sup>a</sup>	
		Nodule type	0.092	
		Radiation dose	0.275	
		Reconstruction algorithm	0.130	
		Reconstruction algorithm* Nodule size	0.287	
5	Nodule size	0.008 <sup>a</sup>		
	Nodule type	0.059		
	Radiation dose	0.275		
	Reconstruction algorithm	0.127		
	Reconstruction algorithm* Nodule type	0.042a		
6	Nodule size	0.156		
	Nodule type	0.231		
	Radiation dose	0.275		
	Reconstruction algorithm	0.005 <sup>a</sup>		
	Nodule size*Nodule type	0.337		
Final model	1	Nodule size	<0.001 <sup>a</sup>	
		Nodule type	0.018a	
		Reconstruction algorithm and Reconstruction algorithm* Nodule type	0.249	iDose <sup>4</sup> compared to FBP; simulated solid nodule
			0.739	IMR compared to FBP; simulated solid nodule
			0.047 <sup>a</sup>	IMR compared to iDose <sup>4</sup> ; simulated solid nodule
			0.375	iDose <sup>4</sup> compared to FBP; simulated GGN
			<0.001 <sup>a</sup>	IMR compared to FBP; simulated GGN
			<0.001 <sup>a</sup>	IMR compared to iDose <sup>4</sup> ; simulated GGN

<sup>a</sup>P < 0.05.

FBP, filtered back projection; IMR, iterative model reconstruction; GGN, ground-glass nodule.

**Supplemental Table 4. Relative attenuation measurement error according to nodule type, various radiation dose protocols, and IR algorithms**

CTDI <sub>vol</sub> (mGy)	Simulated solid nodule (+100 HU)						Simulated GGN (-630, -800 HU)					
	FBP		iDose <sup>d</sup>		IMR		FBP		iDose <sup>d</sup>		IMR	
	Mean <sup>a</sup>	95% CI	Mean <sup>a</sup>	95% CI	Mean <sup>a</sup>	95% CI	Mean <sup>a</sup>	95% CI	Mean <sup>a</sup>	95% CI	Mean <sup>a</sup>	95% CI
0.20	0.34±0.22	0.11, 0.57	0.21±0.12	0.08, 0.34	0.45±0.11	0.33, 0.56	0.03±0.02	0.02, 0.04	0.03±0.02	0.02, 0.04	0.02±0.01	0.01, 0.02
0.38	0.43±0.11	0.32, 0.54	0.34±0.10	0.23, 0.44	0.52±0.11	0.40, 0.63	0.02±0.02	0.01, 0.03	0.02±0.01	0.02, 0.03	0.01±0.01	0.01, 0.02
0.41	0.33±0.12	0.20, 0.46	0.14±0.07	0.06, 0.21	0.28±0.05	0.23, 0.33	0.03±0.02	0.02, 0.05	0.03±0.01	0.02, 0.03	0.01±0.01	0.01, 0.02
0.68	0.11±0.06	0.05, 0.18	0.13±0.05	0.07, 0.18	0.19±0.07	0.11, 0.26	0.02±0.01	0.01, 0.03	0.02±0.01	0.01, 0.03	0.01±0.00	0.01, 0.02
0.81	0.19±0.13	0.06, 0.32	0.15±0.11	0.04, 0.26	0.25±0.05	0.19, 0.30	0.02±0.10	0.02, 0.03	0.03±0.01	0.02, 0.03	0.01±0.01	0.01, 0.02
0.97	0.29±0.13	0.16, 0.43	0.25±0.09	0.15, 0.35	0.38±0.10	0.28, 0.48	0.03±0.01	0.02, 0.03	0.03±0.01	0.02, 0.03	0.02±0.01	0.01, 0.02
1.32	0.07±0.04	0.02, 0.11	0.05±0.03	0.02, 0.07	0.11±0.03	0.08, 0.15	0.02±0.01	0.02, 0.03	0.02±0.01	0.02, 0.03	0.01±0.01	0.01, 0.02
1.95	0.25±0.07	0.17, 0.32	0.25±0.07	0.17, 0.33	0.34±0.03	0.32, 0.37	0.02±0.01	0.01, 0.03	0.02±0.01	0.01, 0.03	0.02±0.01	0.01, 0.02
2.01	0.11±0.05	0.06, 0.16	0.12±0.06	0.05, 0.18	0.20±0.08	0.11, 0.29	0.02±0.01	0.01, 0.03	0.02±0.01	0.01, 0.03	0.02±0.01	0.01, 0.02
3.35	0.09±0.06	0.02, 0.15	0.09±0.04	0.04, 0.13	0.13±0.05	0.08, 0.17	0.04±0.02	0.03, 0.05	0.04±0.02	0.02, 0.05	0.03±0.01	0.02, 0.03
4.04	0.16±0.02	0.13, 0.18	0.15±0.02	0.13, 0.17	0.21±0.02	0.19, 0.22	0.03±0.01	0.03, 0.04	0.03±0.01	0.02, 0.04	0.02±0.01	0.02, 0.03
6.74	0.07±0.03	0.04, 0.11	0.04±0.01	0.03, 0.09	0.11±0.06	0.04, 0.17	0.03±0.01	0.02, 0.04	0.03±0.01	0.02, 0.04	0.02±0.01	0.02, 0.03

<sup>a</sup>Data are presented as mean±standard deviation.  
 IR, iterative reconstruction; HU, Hounsfield unit; GGN, ground-glass nodule; CTDI<sub>vol</sub>, volume CT dose index; FBP, filtered back projection; IMR, iterative model reconstruction; CI, confidence interval.

**Supplemental Table 5. Generalized estimating equations model for the relative attenuation measurement error**

	Model number	Independent variable	P
Initial model	1	Nodule type	0.015 <sup>a</sup>
		Radiation dose	0.437
		Reconstruction algorithm	0.305
		Radiation dose*Reconstruction algorithm	0.437
	2	Nodule type	0.028 <sup>a</sup>
		Radiation dose	0.392
		Reconstruction algorithm	0.161
		Radiation dose*Nodule type	0.647
	3	Nodule type	0.015 <sup>a</sup>
		Radiation dose	0.437
		Reconstruction algorithm	0.287
		Reconstruction algorithm *Nodule type	0.100
	4	Nodule type	0.015 <sup>a</sup>
		Radiation dose	0.437
		Reconstruction algorithm	0.161
Final model	1	Nodule type	<0.001 <sup>a</sup>

<sup>a</sup>P < 0.05.